Liu et al. *NPG Asia Materials* (2022) 14:30
https://doi.org/10.1038/s41427-022-00381-9

NPG Asia Materials

ARTICLE Open Access

Large barocaloric effect in intermetallic $La_{1.2}Ce_{0.8}Fe_{11}Si_2H_{1.86}$ materials driven by low pressure

Yanfeng Liu[1,2], Xinqi Zheng[3], Feixiang Liang[4], Fengxia Hu[4], Qingzhen Huang[5], Zhe Li[6] and Jian Liu[1,2,7]

Abstract

Barocaloric materials are particularly promising for green and efficient solid-state cooling technology because of their great potential in terms of cooling performance. However, intermetallic materials with outstanding barocaloric effects under low hydrostatic pressure are especially lacking, which has severely delayed the development of barocaloric refrigeration. Here, in a rare-earth intermetallic La-Ce-Fe-Si-H, we achieve a giant specific barocaloric temperature change of 8 K per kbar according to direct measurements of the adiabatic temperature change ΔT_{BCE} under hydrostatic pressure, which is confirmed by a phenomenological transition simulation. This barocaloric strength is significantly better than those in previously reported phase-transitioned alloys. By using a cutting-edge in situ neutron diffraction technique operating under simultaneously varying temperature, magnetic field, and hydrostatic pressure, we reveal that the large isotropic transition volume change in La-Ce-Fe-Si-H plays a crucial role in the giant barocaloric effect. Additionally, we employ Landau expansion theory to demonstrate that the high sensitivity of the transition temperature to the applied pressure produces the sizable ΔT_{BCE} in the itinerant electron metamagnetic transition alloys. Our results provide insight into the development of high-performance barocaloric materials and related cooling systems.

Introduction

Novel cooling technologies based on caloric effects have attracted much attention in recent decades as efficient and environmentally friendly alternatives to conventional gas-compression refrigeration[1–3]. In solid-state caloric materials, phase transitions under the application of a magnetic (magnetocaloric effect)[4–6], electric (electrocaloric effect)[7,8], uniaxial stress (elastocaloric effect)[9,10], or hydrostatic pressure (barocaloric effect) field[11–14] lead to changes in entropy and temperature. The main benefits of materials that exhibit the barocaloric effect (BCE) over other caloric materials are related to the high power density in condensed solids and the wide variety of these materials[2,3]. The giant BCE has been extensively reported for a large number of phase-transition materials, such as magnetic shape memory alloys[13,14], antiperovskite compounds[15], plastic crystals[11,16], organic–inorganic hybrids[17,18], ferrielectric ammonium sulfate[19], and natural rubber[20,21]. However, BCE requires high hydrostatic pressure to trigger phase transitions and to generate large adiabatic temperature changes ΔT_{BCE}, which has undoubtedly limited the development of relevant BCE refrigeration devices[2,3]. In addition, metals with high thermal conductivity are preferred for efficient heat transfer between heat-transfer fluid and barocaloric refrigerants. Regardless of the relatively abundant materials exhibiting a significant barocaloric effect, as shown in Fig. 1, more emerging intermetallic materials exhibiting the giant BCE under low pressure are highly sought to promote barocaloric techniques. $NaZn_{13}$-typed La-Fe-Si alloys are of particular interest as high-performance

Correspondence: Jian Liu (liujian@nimte.ac.cn)
[1]CAS Key Laboratory of Magnetic Materials and Devices, and Zhejiang Province Key Laboratory of Magnetic Materials and Application Technology, Ningbo Institute of Materials Technology and Engineering, Chinese Academy of Sciences, Ningbo 315201, P.R. China
[2]University of Chinese Academy of Sciences, 19A Yuquan Rd, Shijingshan District, Beijing 100049, P. R. China
Full list of author information is available at the end of the article

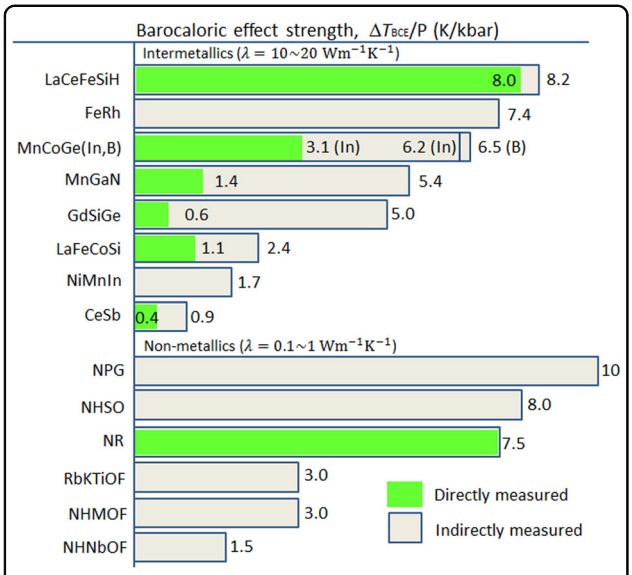

Fig. 1 Comparison of low hydrostatic pressure cooling for selected materials. Barocaloric cooling strength defined as the ratio of the adiabatic temperature change to the applied pressure for typical phase-transitioned intermetallics and non metallics: $La_{1.2}Ce_{0.8}Fe_{11}Si_2H_{1.86}$ (this work), $Fe_{49}Rh_{51}$[46], $MnCoGeB_{0.03}$[47], $MnCoGe_{0.99}In_{0.01}$[48], Mn_3GaN[12], $Gd_5Si_2Ge_2$[26], $LaFe_{11.33}Co_{0.47}Si_{1.2}$[28], $Ni_{49.26}Mn_{36.08}In_{14.66}$[13], CeSb[49], neopentylglycol (marked as NPG)[16], natural rubber (marked as NR)[21], $(NH_4)_2SO_4$ (marked as NHSO)[19], Rb_2KTiOF_5 (marked as RbKTiOF)[17], $(NH_4)_3MoO_3F_3$ (marked as NHMOF)[18], and $(NH_4)_2NbOF_5$ (marked as NHNbOF)[17]. Indirectly measured data were from hydrostatic pressure-dependent differential thermal analysis (DTA)[12,47] and differential scanning calorimetry (DSC)[19,26]. The value of ΔT_{BCE} for different materials is obtained from a low pressure of ~1 kbar, at which condition the barocaloric behavior is almost linear with applied pressure.

magnetocaloric materials[22]. Since the degrees of freedom of the lattice and magnetism in La(Fe,Si)$_{13}$-based alloys coexist and are strongly coupled, both magnetic fields and hydrostatic pressure are capable of driving itinerant electron metamagnetic (IEM) transitions and thus produce magnetocaloric and barocaloric effects. In this study, we focus on a Ce-doped rare-earth-rich $La_{1.2}Ce_{0.8}Fe_{11}Si_2H_{1.86}$, with an off-stoichiometric composition, owing to its strengthened magnetoelastic coupling, as revealed by earlier works[23,24]. Here, we directly measure a giant ΔT_{BCE} of 8 K under a change in hydrostatic pressure of 1 kbar through an IEM transition in the $La_{1.2}Ce_{0.8}Fe_{11}Si_2H_{1.86}$ alloy. The directly measured BCE strength ($\Delta T_{BCE}/\Delta P$) exceeds the corresponding values that have been found for both metallic alloys and non metallics. By combining the changes in hydrostatic pressure, magnetic field, and temperature, we employ advanced in situ neutron scattering measurements under multiple fields to unveil the unique lattice-magnetism coupling mechanism under different stimuli and thus to understand the origin of the remarkable barocaloric effect for the present IEM system. Additionally, a phenomenological calculation based on the Landau expansion model is performed to optimize pressure-sensitive first-order phase transitions and to create a pathway for exploiting promising BCE materials.

Materials and methods

The $La_{1.2}Ce_{0.8}Fe_{11}Si_2$ alloy was prepared by arc melting followed by annealing at 1423 K for 24 h. Slices with thicknesses of ~1.5–2 mm were cut from the parent samples to absorb hydrogen. Hydrogenation was carried out at 573 K under a high purity hydrogen gas atmosphere of 100 kPa for ~5 h to saturate the H concentration. According to the neutron diffraction pattern, the resulting alloy contains mainly the 1:13 phase (~84% in volume fraction) with the chemical composition of $La_{0.57}Ce_{0.43}Fe_{11.68}Si_{1.32}H_{1.86}$ and several secondary phases, i.e., Ce_2Fe_{17} (~7%), La_5Si_3 (~5%), and α-Fe (~4%) (see the "Phase fraction" section in the Supplementary Information). It is known that the α-Fe and La_5Si_3 phases do not exhibit ambient phase transformation and hence do not exhibit the barocaloric effect near room temperature. Ce_2Fe_{17} alloy undergoes spontaneous magnetostriction at ~300 K accompanied by a volume shrinkage of 0.3%[25]. The volume change of Ce_2Fe_{17} is much smaller than that of La(Fe,Si)$_{13}$ alloy (~1.6%). According to the Clausius–Clapeyron equation, the barocaloric effect of Ce_2Fe_{17} alloy is much smaller than that of La(Fe,Si)$_{13}$ alloy. Moreover, the content of the Ce_2Fe_{17} phase is much smaller than that of the La(Fe,Si)$_{13}$ phase in the studied $La_{1.2}Ce_{0.8}Fe_{11}Si_2H_{1.86}$ alloy. Therefore, we believe that the barocaloric performance of the studied $La_{1.2}Ce_{0.8}Fe_{11}Si_2H_{1.86}$ alloy is mainly due to the La(Fe,Si)$_{13}$ phase.

Magnetization measurements were acquired using a vibrating sample magnetometer (VSM, Versalab, Quantum Design) equipped with a beryllium–copper high-pressure cell. The value of the pressure was determined by standard hydraulic press sets equipped with an optional–digital pressure gauge. Thermomagnetization data were recorded at a slow rate of 1.5 K min^{-1} to ensure that the temperature in the pressure cell kept the same pace as the ambient temperature. In-field specific heat measurements were carried out from 0 to 3 T using the heat capacity option of a VersaLab system. For the direct measurement of the adiabatic temperature change of the BCE, a high-pressure hexahedron press was used, where three pairs of symmetrical indenters simultaneously compress the sample from six directions. Cubic pyrophyllite was used as the pressure-transmitting medium to avoid heat exchange. $La_{1.2}Ce_{0.8}Fe_{11}Si_2H_{1.86}$ powders filled the middle of the cubic pyrophyllites, with a PT-1000 thermistor to measure the temperature of the sample during the compression process. The description of the adiabatic temperature change setup is given in the

Supplementary Information. Neutron powder diffraction data on the $La_{1.2}Ce_{0.8}Fe_{11}Si_2H_{1.86}$ sample were collected at the NIST Center for Neutron Research with a high-resolution powder neutron diffractometer (BT1) with monochromatic neutrons of wavelength 0.20774 nm produced by a Ge(311) monochromator. Data were collected in the 2θ range of 14–140° with a step size of 0.05° in the temperature range of 280–350 K, pressure range of 0–6.3 kbar and magnetic field range of 0–7 T. Refinements were carried out using the program GSAS to determine the phase constitution, scaling factor, background, peak shape, atomic positions, thermal vibration factor, and occupancies. The refinement results are given in the 'Neutron powder diffraction section of the Supplementary Information.

Results and discussion

From the curves of field dependences of heat capacity and magnetization in Fig. 2a, b, we can see that the external magnetic field and pressure obviously affect the first-order transition behavior but in an opposite direction for $La_{1.2}Ce_{0.8}Fe_{11}Si_2H_{1.86}$: the thermal-induced IEM transition temperature (T_C) increases under the application of a magnetic field but decreases under hydrostatic pressure. This is reasonable given that the low-temperature ferromagnetic (FM) phase has a higher volume than the high-temperature paramagnetic (PM) phase. The rate of the shift in T_C under a magnetic field (dT_C/dH) is ~3.7 K T^{-1} and under external pressure (dT_C/dP) is ~−26 K $kbar^{-1}$. It should be emphasized that the response of T_C to the application of external pressure in

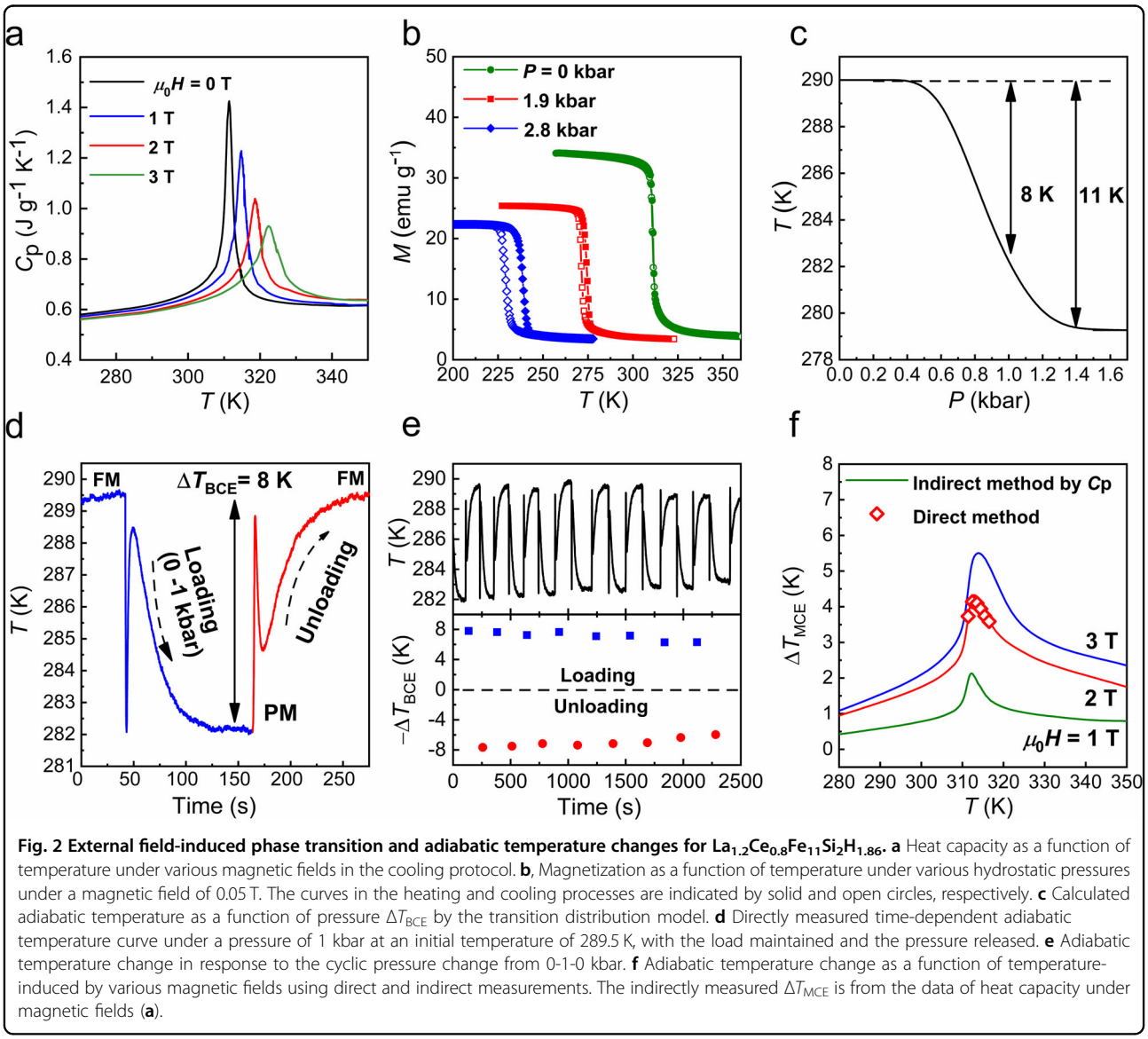

Fig. 2 External field-induced phase transition and adiabatic temperature changes for $La_{1.2}Ce_{0.8}Fe_{11}Si_2H_{1.86}$. **a** Heat capacity as a function of temperature under various magnetic fields in the cooling protocol. **b**, Magnetization as a function of temperature under various hydrostatic pressures under a magnetic field of 0.05 T. The curves in the heating and cooling processes are indicated by solid and open circles, respectively. **c** Calculated adiabatic temperature as a function of pressure ΔT_{BCE} by the transition distribution model. **d** Directly measured time-dependent adiabatic temperature curve under a pressure of 1 kbar at an initial temperature of 289.5 K, with the load maintained and the pressure released. **e** Adiabatic temperature change in response to the cyclic pressure change from 0-1-0 kbar. **f** Adiabatic temperature change as a function of temperature-induced by various magnetic fields using direct and indirect measurements. The indirectly measured ΔT_{MCE} is from the data of heat capacity under magnetic fields (**a**).

our sample is more sensitive than those for other magnetostructural transition alloys, e.g., Mn-Ga-N (−6.5 K kbar^{-1})[12], Gd-Si-Ge (−3.5 K kbar^{-1})[26], Ni-Mn-In (+1.8 K kbar^{-1})[13], stoichiometric La(Fe,Mn,Si)$_{13}$ (−13.9 K kbar^{-1})[27], and La(Fe,Co,Si)$_{13}$ (−9.4 K kbar^{-1})[28]. For IEM systems, T_C is determined by the band structure near the Fermi surface. In the case of the studied $La_{1.2}Ce_{0.8}Fe_{11}Si_2H_{1.86}$ alloy, the hydrostatic pressure shortens the exchange of the 3*d* electrons of Fe atoms and thus affects the band structure near the Fermi surface. Therefore, the nature of the first-order transition strengthens, and the transition hysteresis increases with applied hydrostatic pressure (0.5 K for 0 kbar, 3 K for 1.9 kbar, and 9 K for 2.8 kbar), as shown in Fig. 2b. Importantly, such an ultrahigh sensitivity indicates that low pressure is expected to trigger the IEM transition and thus generate a giant adiabatic temperature change (ΔT_{BCE}) in our sample.

First, we theoretically evaluate how the sample cools during adiabatic pressurization using a phenomenological simulation called the "transition distribution model". This convergence method has been employed to approach the real cooling behavior for MCE materials by analyzing the controlling parameters of phase transitions[5]. Analogous to the magnetic field, we show the change in temperature influenced by pressure. Details of mathematical deduction can be seen in the section "Transition distribution model under pressure" of the Supplementary Information. As shown in Fig. 2c, at the initial temperature of 290 K, the sample maintains the FM state when the pressure is lower than 0.4 kbar and then starts to undergo the FM-PM transition. The magnetostructural transition is completed with pressurization up to 1.4 kbar, resulting in a maximum ΔT_{BCE} of 11 K. More strikingly, a giant BCE strength of $\Delta T_{BCE} = 8$ K at 1 kbar is achieved by fulfilling a phase transition fraction of ~80%. Such an exceptional ΔT_{BCE} under low pressure has also been verified by pressure-dependent calorimetric measurement with the quasi-direct method (described in the section "DSC under pressure" in the Supplementary Information).

As a straightforward assessment of BCE, a direct measurement of the adiabatic temperature change upon the rapid application and removal of hydrostatic pressure was carried out (see the section "Description of direct ΔT_{BCE} measurements" in the Supplementary Information). The time-dependent temperature change is presented in Fig. 2d. Upon the application of a pressure of 1 kbar within 50 s, the sample cools from 290 to 282 K, causing a large ΔT_{BCE} of 8 K. Then, it remains at a nearly constant temperature for 70 s when the pressure is maintained, indicating very good adiabatic pressurization conditions that guarantee the accuracy of the measured ΔT_{BCE} in this experiment. Upon the release of pressure, the sample heats back to the initial temperature. This confirms the reversibility of the phase transition and BCE temperature variation. It should be noted that the sharp temperature peaks prior to BCE are due to the signal from the temperature sensor subjected to the applied pressure. The directly achieved temperature change is highly consistent with the theoretically predicted value from the aforementioned phenomenological model, as well as the results from quasi-direct measurements. Furthermore, the influence of pressure cycles on ΔT_{BCE} is measured. Although for each cycle the giant temperature change exhibits good recoverability (a symmetric rise and drop in temperature), there is a slight degradation of the absolute value of ΔT_{BCE} down to 6 K under pressurization-depressurization cycles (Fig. 2e). Such energy losses could be ascribed to mechanical friction at particle and grain boundaries[29], which might be overcome by lattice tuning and microstructural optimization[30,31].

For comparison to the BCE, the magnetic field-induced adiabatic temperature change (ΔT_{MCE}) was investigated by direct and indirect measurements based on heat capacity data. As shown in Fig. 2f, under a magnetic field of 2 T, which in general is accessible with permanent magnets, the maximum ΔT_{MCE} is approximately +4 K, which is only half of the value of the ΔT_{BCE} generated by 1 kbar pressure (Fig. 2f). This comparison clearly reveals that relatively low pressure is prone to producing a more significant caloric effect than a magnetic field is for our $La_{1.2}Ce_{0.8}Fe_{11}Si_2H_{1.86}$ refrigerant.

From the Clausius–Clapeyron equation, the ΔT_{BCE} in a complete first-order phase transition can be determined by the crucial parameters of (i) the volume change of transition $\Delta\omega$ and (ii) the sensitivity of the transition temperature to applied pressure dT_C/dP:

$$\Delta T_{BCE} = \frac{T}{C_p}\Delta S_{BCE} = \frac{T}{C_p}\frac{V\Delta\omega}{\rho}\left(\frac{dT_c}{dP}\right)^{-1} \quad (1)$$

where T is the temperature, P the pressure, C_p the heat capacity, V the volume, and ρ the density. Both $\Delta\omega$ and dT_C/dP are strongly dependent on magnetostructural coupling[12]. To obtain experimental insight into the physical mechanism of the field-triggered IEM transition and particularly to examine the bond structural changes, cutting-edge neutron scattering measurements were carried out as a function of pressure, magnetic field, and temperature (Fig. 3a). The collected diffraction spectrum shows the shift in the diffraction peaks, which indicates that the sample undergoes complete phase transitions under different fields.

The crystallographic structure of La-Fe-Si-based compounds is described as a CsCl-type packing of rare-earth atoms and Fe-I centered icosahedra (Fig. 3a). La/Ce atoms occupy the 8a sites, and the Fe-I sites at 8b are fully occupied by Fe atoms. Each Fe-I atom is surrounded by an icosahedron of 12 Fe-II atoms at 96i, which is randomly

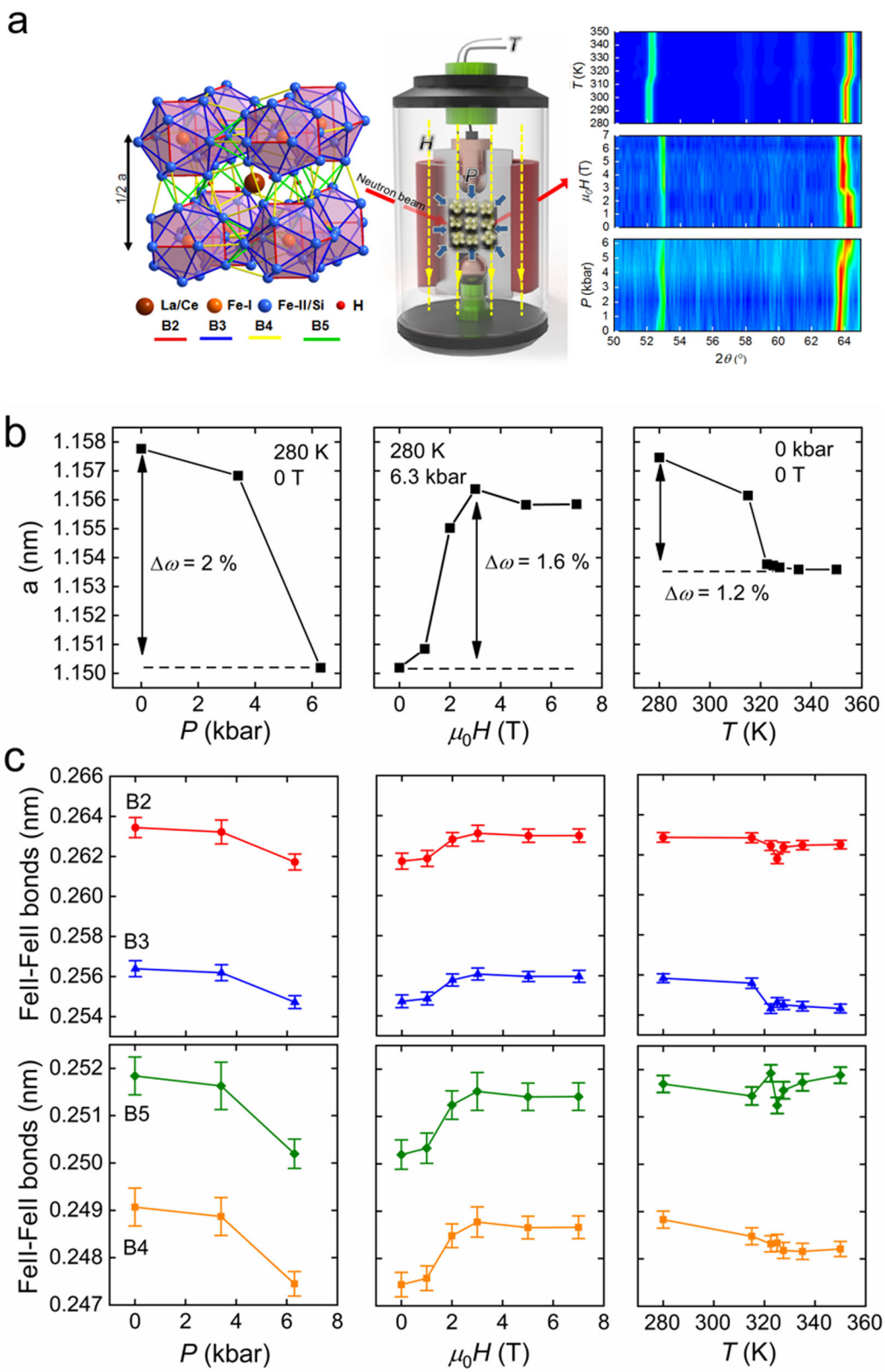

Fig. 3 Changes in lattice structure under different external stimuli. a Schematic of the La-Ce-Fe-Si-H crystallographic structure, in situ neutron diffraction device, and collected diffraction spectrum under different fields (from left to right). **b** Lattice parameters as functions of hydrostatic pressure, magnetic field, and temperature. **c** Multifield dependence of the Fe-Fe bond length in a unit cell.

occupied by Si and Fe atoms. The icosahedra centered by the Fe-I site are interconnected with adjacent icosahedra rotated 90° by the Stella quadrangular. H interstitials enter the 48 f site, an octahedral site with 4 Fe-II/Si and 2 La/Ce nearest neighbors[32]. The lattice exhibits a discontinuity in the magnetic ordering. As shown in Fig. 3b, the sample remains in the PM state under a pressure of 3.4 kbar. However, the pressure-dependent thermomagnetization data (Fig. 2b) indicate that 3.4 kbar pressure is sufficient to fully induce the transition at 280 K. Such an inconsistency is very likely because the actual pressure value on the powder sample is less than the calculated pressure in the high-pressure neutron diffraction experiment. During the pressurization process, some particles of the sample inevitably fill in the tiny gap between the rig and pressurized cylinder of the high-pressure units in the neutron diffraction device. The resultant large friction offsets a considerable part of the pressure, and thus, the pressure might be overestimated. Therefore, the pressure-dependent neutron diffraction experiment can only be used to qualitatively discuss the difference in the effects of pressure, magnetic field, and temperature on lattice structure and bond length.

The application of a nominal pressure of 6.3 kbar at 280 K drives the sample to undergo the FM-PM transition and produces a giant $\Delta\omega$ of 2%. Such a volume change consists of two parts: shrinkage by phase transition and normal elastic volume compression. Using the bulk elastic modulus of 2.29×10^3 kbar taken from the close composition of $LaFe_{11}Si_2$[33], the volume change by the compression effect is calculated to be 0.3%. Therefore, the dominant contribution to the total volume change can be ascribed to the magnetostructural transition (~1.7%). In comparison, the application of a magnetic field leads to a volume change of 1.6% in the phase transitions, which is similar to the volume change caused by hydrostatic pressure. However, the temperature-induced volume change is detected to be an even smaller value of 1.2%.

To understand the discrepancy in volume change induced by different external stimuli, we employ general local-moment volume magnetostriction theory in the framework of the Callen-Callen model[34]. The volume magnetostriction $\Delta\omega$ on the IEM transition is proportional to the squared magnetization ΔM^2, compressibility k, and magnetoelastic coupling coefficient C_{mv}, while it is negatively proportional to the squared thermal spin fluctuations $\Delta\xi^2$:

$$\Delta\omega(T_C) = kC_{\mathrm{mv}}\left\{\Delta M(T_C)^2 - \Delta\xi(T_C)^2\right\} \quad (2)$$

Here, $\Delta\xi^2$is proportional to the squared temperature. Considering that the temperature range in our in situ neutron diffraction experiment is quite narrow, the contribution from $\Delta\xi^2$ to the volume change is similar under different external stimuli. Therefore, the large transition volume change triggered by external fields is mainly ascribed to the change in the local magnetic moment. For La-Fe-Si-based alloys, ferromagnetism originates from the exchange interaction of the 3*d* itinerant electrons of Fe-II atoms[35]. In $La(Fe,Si)_{13}$-based alloys, the shortened bond length between the Fe atoms weakens the ferromagnetic coupling between Fe atoms and therefore lowers the magnetization of the alloy. Compared with the bonds between Fe-I and Fe-II atoms, the lengths of Fe-II - Fe-II bonds (marked as B2, B3, B4, and B5) are the determining factors in mastering the magnetic moment[36]. With an in-depth investigation of the fine structure of $La_{1.2}Ce_{0.8}Fe_{11}Si_2H_{1.86}$ by in situ neutron diffraction methods, we can see that the Fe-II - Fe-II bonds display the most significant shrinkage, by 0.66 and 0.53% with the application of pressure and magnetic field, respectively (Fig. 3c). It should be clarified that the difference in bond length changes under hydrostatic pressure and the magnetic field is due to the compression effect of hydrostatic pressure and experimental error. The field-dependent neutron diffraction results indicate that the symmetry of the icosahedra in the $La_{1.2}Ce_{0.8}Fe_{11}Si_2H_{1.86}$ alloy remains constant during the IEM transition triggered by external hydrostatic pressure and magnetic field. Interestingly, in terms of the thermal phase transition, the icosahedron cluster is deformed. In the case of the temperature-driven PM-FM transition, however, the B4 bond varies by a much smaller magnitude, 0.2%, and the B5 bond remains nearly unchanged. In addition, the B2 bond changes by a smaller magnitude (0.1%) than B3 (0.55%). Since the IEM transition is closely related to the distance-dependent exchange, the deformation of the cluster could cause weakening of the IEM transition[37]. Thus, we assume that the small value of $\Delta\omega$ in the thermally triggered phase transition is very likely due to its lattice distortion. In other words, the application of pressure and magnetic field are assumed to induce a more drastic change in the magnetic moment and to drive a larger phase transition volume change than the temperature.

After investigating the impact of $\Delta\omega$ on the BCE, we discuss another important parameter, dT_C/dP, for the enhancement of ΔT_{BCE}. The pressure dependence of the transition temperature is regarded as an approximate measure of the stability of the ordered state against pressure[12]. Assuming an ideal condition of infinite pressure in Eq. (1), ΔT_{BCE} varies inversely with dT_C/dP. However, the real phase transition occurs in a finite temperature range rather than at a specific temperature. In the case of a small dT_C/dP, it is extraordinarily difficult to complete phase transition at low pressure, and thus the obtained ΔT_{BCE} is significantly smaller than the upper bound of ΔT_{BCE}. Similar to magnetocaloric materials[38], the magnitude of dT_C/dP must be at an optimal value to

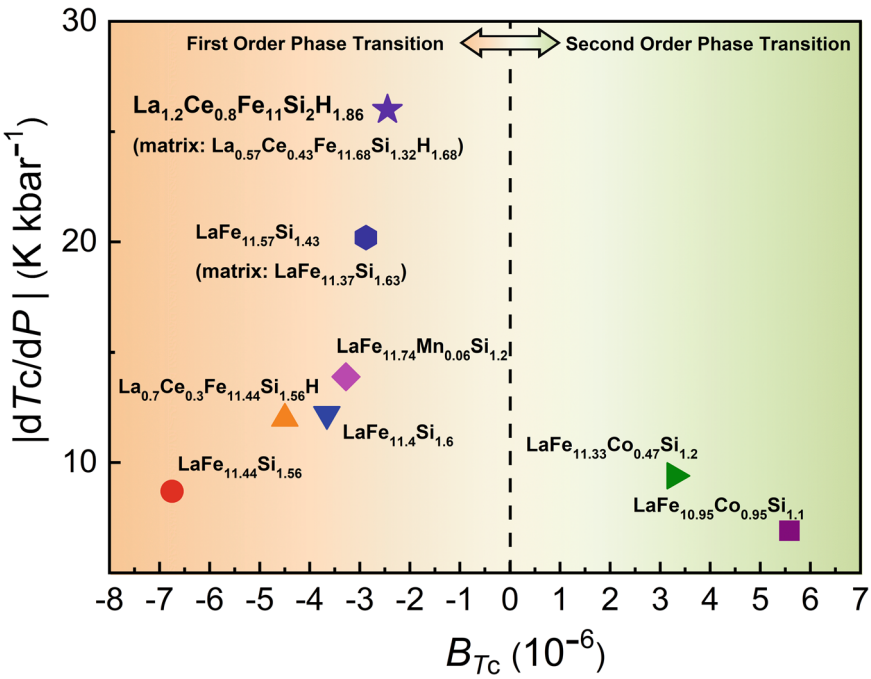

Fig. 4 Pressure-sensitive phase transition. The ratio of the transition temperature to applied pressure related to the secondary Landau coefficient at T_C for selected La-Fe-Si IEM alloys: $La_{1.2}Ce_{0.8}Fe_{11}Si_2H_{1.86}$ (this work), $LaFe_{11.33}Co_{0.47}Si_{1.2}$[28], $LaFe_{11.74}Mn_{0.06}Si_{1.2}$[25], $LaFe_{11.44}Si_{1.56}$[43], $LaFe_{11.4}Si_{1.6}$[39], $LaFe_{11.57}Si_{1.43}$[44], $LaFe_{10.95}Co_{0.95}Si_{1.1}$[45], and $La_{0.7}Ce_{0.3}Fe_{11.44}Si_{1.56}H$[34]. B_{Tc} is calculated from the magnetization curve at T_C using the Landau expansion theory.

maximize ΔT_{BCE} under limited pressure. It must be noted that most of the available room temperature BCE material systems exhibit a relatively small dT_C/dP that needs to be critically improved to achieve a larger BCE under low pressure. As modulating the IEM transition order has been proposed as a feasible way to increase dT_C/dP and to reduce the strength of the required driving pressure[39], we attempt to explore the potential of dT_C/dP based on the IEM transition model.

According to Landau's theory, the slope of the H/M-M^2 curve (Arrott curve) is nearly equal to $B(T)$. Therefore, the secondary Landau coefficient $B(T_C)$, similar to the Arrott curve, can be used as the basis for judging the transition order of the La(Fe,Si)$_{13}$-based alloys[40]. Generally, a negative $B(T_C)$ leads to a first-order phase transition, and a positive $B(T_C)$ corresponds to a second-order phase transition[41]. By taking the influence of spin fluctuations and magnetoelastic coupling into account, the Landau expansion theory can describe the IEM transition behavior under hydrostatic pressure well: the pressure dependence of T_C around zero pressure is maximized when the secondary Landau coefficient B at T_C approaches zero[42]. We derived the value of B at T_C by fitting the magnetization data for reported La-Fe-Si-based alloys (described in the section "Landau expansion model" in the Supplementary Information). As plotted in Fig. 4, the magnitude of dT_C/dP for La-Fe-Si alloys in the literature varies from 6 to 22 K kbar^{-1} owing to the scattered B at Tc far from zero[25,28,34,39,43–45]. For the present work, we manipulate the IEM transition by simultaneously introducing large Ce atoms and interstitial H atoms. Consequently, the studied composition of $La_{1.2}Ce_{0.8}Fe_{11}Si_2H_{1.86}$ is near the boundary of the phase transition, where the value of B at Tc is rather small. Such a unique phase-transition feature indicates that our $La_{1.2}Ce_{0.8}Fe_{11}Si_2H_{1.86}$ alloy simultaneously possesses both a giant volume change and small hysteresis, especially under low pressure. Thus, low pressure of ~1 kbar can convert a large phase fraction of almost 80%, leading to a giant reversible ΔT_{BCE} of 8 K.

Conclusions

From the present findings, we demonstrate that giant barocaloric performance at low pressure can be realized by enhancing the transition volume change $\Delta\omega$ and manipulating the pressure-sensitive phase transitions dTc/dP. Both crucial parameters are closely related to the magnetoelastic coupling coefficient. In this sense, the strengthening of magnetoelastic coupling is one key step for developing more efficient BCE materials. This criterion goes beyond La-Fe-Si IEM-type alloys and should be applicable to other first-order transition materials.

Acknowledgements
This work is supported by the National Key Research and Development Program of China (2021YFB3501203), the Ningbo Science and Technology Innovation 2025 Major Project (2020Z063), the International Partnership Program of the Chinese Academy of Sciences (Grant No. 174433KYSB20180040), the National Natural Science Foundation of China (51971232), and the Zhejiang Provincial Natural Science Foundation of China (LD21E010001). We thank A. Planes and L. Mañosa for providing helpful suggestions.

Author details
[1]CAS Key Laboratory of Magnetic Materials and Devices, and Zhejiang Province Key Laboratory of Magnetic Materials and Application Technology, Ningbo Institute of Materials Technology and Engineering, Chinese Academy of Sciences, Ningbo 315201, P.R. China. [2]University of Chinese Academy of Sciences, 19A Yuquan Rd, Shijingshan District, Beijing 100049, P. R. China. [3]School of Materials Science and Engineering, University of Science and Technology Beijing, Beijing 100083, P. R. China. [4]Beijing National Laboratory for Condensed Matter Physics & State Key Laboratory of Magnetism, Institute of Physics Chinese Academy of Sciences, Beijing 100190, P. R. China. [5]NIST Center for Neutron Research, National Institute of Standards and Technology, Gaithersburg, MD 20899, USA. [6]Center for Magnetic Materials and Devices & Key Laboratory for Advanced Functional and Low Dimensional Materials of Yunnan Higher Education Institute, Qujing Normal University, Qujing 655011, P. R. China. [7]Center of Materials Science and Optoelectronics Engineering, University of Chinese Academy of Sciences, Beijing 100049, P.R. China

Author contributions
JL conceived the idea. Y.L., fabricated the samples. Y.L., X.Z., F.L., F.H., Q.H., and Z.L. conducted the experiments and data analysis. YL and JL wrote the manuscript. All authors were involved in the discussion of the results and commented on the paper.

Conflict of interest
The authors declare no competing interests.

Publisher's note
Springer Nature remains neutral with regard to jurisdictional claims in published maps and institutional affiliations.

Supplementary information The online version contains supplementary material available at https://doi.org/10.1038/s41427-022-00381-9.

Received: 24 February 2021 Revised: 23 January 2022 Accepted: 14 March 2022.
Published online: 8 April 2022

References

1. Moya, X., Kar-Narayan, S. & Mathur, N. D. Caloric materials near ferroic phase transitions. *Nat. Mater.* **13**, 439–450 (2014).
2. Manosa, L. & Planes, A. Materials with giant mechanocaloric effects: cooling by strength. *Adv. Mater.* **29**, 1603607 (2017).
3. Manosa, L. & Planes, A. Solid-state cooling by stress: a perspective. *Appl. Phys. Lett.* **116**, 050501 (2020).
4. Krenke, T. et al. Inverse magnetocaloric effect in ferromagnetic Ni–Mn–Sn alloys. *Nat. Mater.* **4**, 450–454 (2005).
5. Liu, J., Gottschall, T., Skokov, K. P., James, D. M. & Gutfleisch, O. Giant magnetocaloric effect driven by structural transitions. *Nat. Mater.* **11**, 620–626 (2012).
6. Campos, A. et al. Ambient pressure colossal magnetocaloric effect tuned by composition in $Mn_{1-x}Fe_xAs$. *Nat. Mater.* **5**, 802–804 (2006).
7. Mischenko, A. S., Zhang, Q., Scott, J. F., Whatmore, R. W. & Mathur, N. D. Giant electrocaloric efect in thin-flm $PbZr_{0.95}Ti_{0.05}O_3$. *Science* **311**, 1270–1271 (2006).
8. Neese, B. et al. Large electrocaloric effect in ferroelectric polymers near room temperature. *Science* **321**, 821–823 (2008).
9. Bonnot, E., Romero, R., Manosa, L., Vives, E. & Planes, A. Elastocaloric effect associated with the martensitic transition in shape-memory alloys. *Phys. Rev. Lett.* **100**, 125901 (2008).
10. Hou, H. et al. Fatigue-resistant high-performance elastocaloric materials made by additive manufacturing. *Science* **29**, 1116–1121 (2019).
11. Li, B. et al. Colossal barocaloric effects in plastic crystals. *Nature* **567**, 506–510 (2019).
12. Matsunami, D., Fujita, A., Takenaka, K. & Kano, M. Giant barocaloric effect enhanced by the frustration of the antiferromagnetic phase in Mn_3GaN. *Nat. Mater.* **14**, 73–78 (2015).
13. Manosa, L. et al. Giant solid-state barocaloric effect in the Ni–Mn–In magnetic shape-memory alloy. *Nat. Mater.* **9**, 478–481 (2010).
14. Aznar, A. et al. Giant barocaloric effect in all-d-metal Heusler shape memory alloys. *Phys. Rev. Mater.* **3**, 044406 (2019).
15. Bermudez-Garcia, J. M. et al. Giant barocaloric effect in the ferroic organic-inorganic hybrid [TPrA][Mn(dca)3] perovskite under easily accessible pressures. *Nat. Commun.* **8**, 15715 (2017).
16. Lloveras, P.et. al. Colossal barocaloric effects near room temperature in plastic crystals of neopentylglycol. *Nat. Commun.* **10**, 1803 (2019).
17. Gorev, M. V., Bogdanov, E. V., Flerov, I. N., Voronov, V. N. & Laptash, N. M. Barocaloric effect in oxyfluorides Rb_2KTiOF_5 and $(NH_4)_2NbOF_5$. *Ferroelectrics* **397**, 76–80 (2010).
18. Flerov, I. N., Gorev, M. V., Tressaud, A. & Laptash, N. M. Perovskite-like fluorides and oxyfluorides: phase transitions and caloric effects. *Crystallogr. Rep.* **56**, 9–17 (2011).
19. Lloveras, P. et al. Giant barocaloric effects at low pressure in ferrielectric ammonium sulphate. *Nat. Commun.* **6**, 8801 (2015).
20. Carvalho, A. M. G., Imamura, W., Usuda, E. O. & Bom, N. M. Giant room-temperature barocaloric effects in PDMS rubber at low pressures. *Eur. Polym. J.* **99**, 212–221 (2018).
21. Bom, N. M., Usuda, E. O., Guimaraes, G. M., Coelho, A. A. & Carvalho, A. M. G. Note: experimental setup for measuring the barocaloric effect in polymers: application to natural rubber. *Rev. Sci. Instrum.* **046103**, 88 (2017).
22. Hu, F., Shen, B., Sun, J. & Cheng, Z. Influence of negative lattice expansion and metamagnetic transition on magnetic entropy change in the compound $LaFe_{11.4}Si_{1.6}$. *Appl. Phys. Lett.* **78**, 3675–3677 (2001).
23. Zhang, M., Liu, J., He, C. & Yan, A. Novel microstructure and large magnetocaloric effect in $La_2Fe_{11}Si_2$ magnetic refrigerant. *Mater. Lett.* **134**, 87–90 (2014).
24. Yang, J. The influence of Ce substitution on microstructure, phase formation and magnetocaloric properties in off-stoichiometric La2-xCexFe11Si2 alloys. *Intermetallics* **103**, 97–100 (2018).
25. Andreev, A. V. & Lindbaum, A. Spontaneous magnetostriction of Ce_2Fe_{17}. *J. Alloy. Compd.* **297**, 43–45 (2000).
26. Yuce, S. et al. Barocaloric effect in the magnetocaloric prototype $Gd_5Si_2Ge_2$. *Appl. Phys. Lett.* **101**, 071906 (2012).
27. Lovell, E. et al. The $La(Fe,Mn,Si)_{13}H_z$ magnetic phase transition under pressure. *Phys. Status Solidi Rrl.* **11**, 1700143 (2018).
28. Manosa, L. et al. Inverse barocaloric effect in the giant magnetocaloric La–Fe–Si–Co compound. *Nat. Commun.* **2**, 595 (2011).
29. Zhao, D., Liu, J., Feng, Y., Sun, W. & Yan, A. Giant elastocaloric effect and its irreversibility in [001]-oriented $Ni_{45}Mn_{36.5}In_{13.5}Co_5$ meta-magnetic shape memory alloys. *Appl. Phys. Lett.* **110**, 021906 (2017).
30. Li, Y. et al. Energy-efficient elastocaloric cooling by flexibly and reversibly transferring interface in magnetic shape-memory alloys. *ACS Appl. Mater. Interfaces* **10**, 25438 (2018).
31. Lyubina, J., Schafer, R., Martin, R., Schultz, R. & Gutfleisch, R. Novel design of La(Fe,Si)$_{13}$ alloys towards high magnetic refrigeration performance. *Adv. Mater.* **22**, 3735–3739 (2010).
32. Shao, Y., Lu, B., Zhang, M. & Liu, J. An X-ray absorption spectroscopy study of La-Fe-Si-(H) magnetocaloric alloys. *Acta Mater.* **150**, 206–212 (2018).
33. Wang, F. et al. Strong interplay between structure and magnetism in the giant magnetocaloric intermetallic compound LaFe11.4Si1.6: a neutron diffraction study. *J. Phys. Condens. Matter* **15**, 5269–5278 (2003).
34. Fujieda, S., Fujita, A. & Fukamichi, K. Strong pressure effect on the Curie temperature of itinerant-electron metamagnetic $La(Fe_{0.88}Si_{0.12})_{13}H_y$ and $La_{0.7}Ce_{0.3}(Fe_{0.88}Si_{0.12})_{13}H_y$. *Mater. Trans.* **50**, 483–486 (2009).
35. Bao, L. et al. Magnetocaloric properties of La(Fe,Si)13-based material and its hydride prepared by industrial mischmetal. *Appl. Phys. Lett.* **101**, 162406 (2012).
36. Rosca, M. et al. Neutron diffraction study of $LaFe_{11.31}Si_{1.69}$ and $LaFe_{11.31}Si_{1.69}H_{1.45}$ compounds. *J. Alloy. Compd.* **490**, 59–55 (2010).
37. Gruner, M. et al. Moment-volume coupling in $La(Fe_{1-x}Si_x)_{13}$. *Phys. Status Solidi* **255**, 1700465 (2018).
38. Sandeman, K. G. Magnetocaloric materials: the search for new systems. *Scr. Mater.* **67**, 566–571 (2012).

39. Karpenkov, D. et al. Pressure dependence of magnetic properties in $La(Fe,Si)_{13}$: multistimulus responsiveness of caloric effects by modeling and experiment. *Phys. Rev. Appl.* **13**, 034014 (2020).
40. Gu, K., Li, J., Ao, W., Jian, Y. & Tang, J. The magnetocaloric effect in $(Dy,Tb)Co_2$ alloys. *J. Alloy. Compd.* **441**, 39–42 (2007).
41. Inoue, J. & Shimizu, M. Volume dependence of the first-order transition temperature for RCo_2 compounds. *J. Phys. F: Met. Phys.* **12**, 1811 (1982).
42. Fujita, A., Fujieda, S. & Fukamichi, K. Influence of hydrogenation on volume dependence of the Curie temperature and entropy change in $La(Fe_{0.86}Si_{0.14})_{13}$. *J. Phys: Conf. Ser.* **200**, 092006 (2010).
43. Fujita, A., Fukamichi, K. & Goto, T. Concentration dependence of pressure effect in $La(Fe_xSi_{1-x})_{13}$ compounds. *Mater. Trans.* **47**, 478–484 (2006).
44. Lyubina, J., Nenkov, K., Schultz, L. & Gutfleisch, O. Multiple metamagnetic transitions in the magnetic refrigerant $La(Fe, Si)_{13}H_x$. *Phys. Rev. Lett.* **101**, 177203 (2008).
45. Hao, J. Z. et al. Large enhancement of magnetocaloric and barocaloric effects by hydrostatic pressure in $La(Fe_{0.92}Co_{0.08})_{11.9}Si_{1.1}$ with a $NaZn_{13}$-type structure. *Chem. Mater.* **32**, 1807–1818 (2020).
46. Stern-Taulats, E. et al. Reversible adiabatic temperature changes at the magnetocaloric and barocaloric effects in $Fe_{49}Rh_{51}$. *Appl. Phys. Lett.* **107**, 152409 (2015).
47. Aznar, A. et al. Giant and reversible inverse barocaloric effects near room temperature in ferromagnetic $MnCoGeB_{0.03}$. *Adv. Mater.* **31**, 1903577 (2019).
48. Wu, R. et al. Giant barocaloric effect in hexagonal Ni_2In-type Mn-Co-Ge-In compounds around room temperature. *Sci. Rep.* **5**, 180207 (2015).
49. Strassle, T., Furrer, A., Hossain, Z. & Geibel, C. Magnetic cooling by the application of external pressure in rare-earth compounds. *Phys. Rev. B* **67**, 054407 (2003).